The Astronomical Journal, 137:5120–5133, 2009 June doi:10.1088/0004-6256/137/6/5120
© 2009. The American Astronomical Society. All rights reserved. Printed in the U.S.A.

PROBING SPECTROSCOPIC VARIABILITY OF GALAXIES AND NARROW-LINE ACTIVE GALACTIC NUCLEI IN THE SLOAN DIGITAL SKY SURVEY

C. W. Yip[1], A. J. Connolly[2], D. E. Vanden Berk[3], R. Scranton[4], S. Krughoff[2], A. S. Szalay[1], L. Dobos[5], C. Tremonti[6], M. Taghizadeh-Popp[1], T. Budavári[1], I. Csabai[5], R. F. G. Wyse[1], and Ž. Ivezić[2]
[1] Department of Physics and Astronomy, The Johns Hopkins University, 3701 San Martin Drive, Baltimore, MD 21218, USA
[2] Astronomy Department, University of Washington, Seattle, WA 98195, USA
[3] Saint Vincent College, 300 Fraser Purchase Road, Latrobe, PA 15650, USA
[4] Department of Physics, University of California, Davis, CA 95616, USA
[5] Department of Physics of Complex Systems, Eötvös Loránd University, H-1117 Budapest, Hungary
[6] Max-Planck-Institut für Astronomie, Königstuhl 17, D-69117, Heidelberg, Germany
Received 2008 November 24; accepted 2009 March 29; published 2009 May 12

ABSTRACT

Under the unified model for active galactic nuclei (AGNs), narrow-line (Type 2) AGNs are, in fact, broad-line (Type 1) AGNs but each with a heavily obscured accretion disk. We would therefore expect the optical continuum emission from Type 2 AGNs to be composed mainly of stellar light and nonvariable on the timescales of months to years. In this work we probe the spectroscopic variability of galaxies and narrow-line AGNs using the multiepoch data in the Sloan Digital Sky Survey Data Release 6. The sample contains 18,435 sources for which there exist pairs of spectroscopic observations (with a maximum separation in time of $\sim$ 700 days) covering a wavelength range of 3900–8900 Å. To obtain a reliable repeatability measurement between each spectral pair, we consider a number of techniques for spectrophotometric calibration resulting in an improved spectrophotometric calibration of a factor of 2. From these data we find no obvious continuum and emission-line variability in the narrow-line AGNs on average—the spectroscopic variability of the continuum is 0.07 ± 0.26 mag in the g band and, for the emission-line ratios $\log_{10}$([N II]/Hα) and $\log_{10}$([O III]/Hβ), the variability is 0.02 ± 0.03 dex and 0.06 ± 0.08 dex, respectively. From the continuum variability measurement we set an upper limit on the ratio between the flux of the varying spectral component, presumably related to AGN activities, and that of the host galaxy to be $\sim$ 30%. We provide the corresponding upper limits for other spectral classes, including those from the BPT diagram, eClass galaxy classification, stars, and quasars.

Key words: galaxies: general – techniques: spectroscopic

1. INTRODUCTION

Active galactic nuclei (AGNs) are found to vary in the time domain at many frequencies. The underlying physical mechanism driving the variability seen in AGN spectra is unknown (e.g., Peterson 2001; Bono et al. 2003). Several scenarios have been proposed including accretion disk instability (Kawaguchi et al. 1998), supernova explosions (Aretxaga et al. 1997), microlensing by stars in the intervening galaxy (Hawkins 1993), and varying ionizing source and/or varying optical depth of the material in the vicinity of light-generating regions (e.g., Tohline & Osterbrock 1976; Goodrich 1989). At present, models involving nonthermal emission from the jets or events occurring on the AGN accretion disk are most favored (see, e.g., Stalin et al. 2004, for a summary of variability models in AGNs by radio loudness).

Most variability studies, however, have been focused on Type 1 (broad-line) AGNs. While the emission lines of Type 2 (narrow-line) AGNs were found to vary in the X-rays on timescales from hours to years (Guainazzi et al. 1998; Mueller et al. 2003; Mateos et al. 2007), their optical continua and emission lines are generally considered to be nonvariable. For the emissions from the narrow-line regions, the spatially low-density region (electron density $n_e \sim 1,000$ cm^{-3}) results in a long ($\sim$ 100 years) recombination time[7] (Peterson et al. 1995), exceeding the duration of a typical observation. For the optical continuum, it is commonly considered to be composed mainly of the stellar light, in accordance with the expectation from the unification model (Antonucci 1993; Urry & Padovani 1995) in which Type 2 objects are obscured by a dusty torus along the line-of-sight. Dominated by the stellar light, the optical continuum in Type 2 AGNs should therefore be temporally nonvariable. There is, however, no strong observational evidence in the time domain to either support or dispute these ideas.

From a four-year monitoring of the broad-band optical variability of 35 Type 1 and 2 Seyfert galaxies, Winkler et al. (1992) demonstrated that most galaxies in their sample were variable. Another promising work to probe Type 2 AGN variability in the optical was the intra-night variability of Seyfert 2 galaxies observed by Jang (2001), where two out of the three objects varied by $\sim$ 0.25 mag. Further, Trippe et al. (2008) found a Type 1.9 Seyfert galaxy (Osterbrock 1989) to change into a Type 2 Seyfert over a few years, and proposed the underlying cause to be a varying ionizing continuum.

The UV-optical variability of broad-line AGNs is better established with an amplitude of $\sim$ 10% (e.g., see discussions in Vanden Berk et al. 2004). Wavelength dependence of QSO variability has been studied by Wilhite et al. (2005), and the C IV-emission dependence by Wilhite et al. (2006) in the Sloan Digital Sky Survey (SDSS; York et al. 2000). In these studies the authors have developed a method to remove wavelength-dependent systematics which may exist in the spectra, from a spectroscopic plate[8] at one epoch of observation to the same plate at another epoch. Correcting for this on a plate-to-plate

[7] The recombination time τ_e is referred to that of the hydrogen atom, so that $\tau_e = 1/(n_e\,\alpha_A)$, where n_e is the electron density. The total recombination coefficient of hydrogen, α_A, is equal to 4.18×10^{-13} cm^3 s^{-1} at an electronic temperature $T_e = 10^4$ K (Osterbrock 1989).

[8] A spectroscopic plate in the SDSS contains a set of spectra which are observed simultaneously.

basis, they were able to select variable QSOs and to demonstrate a power-law-like QSO difference spectrum, which in turn can be explained by the change in the accretion rate in the thermal accretion disk (Pereyra et al. 2006). QSO photometric variability in the SDSS has been studied by Vanden Berk et al. (2004) for its dependence on physical parameters such as redshift, luminosity, and radio properties; by de Vries et al. (2003) in which the authors used both the SDSS and the historical observations (up to $\sim$ 50 years) and found the timescale of the variability to be $\sim$ 2 years; and by Ivezić et al. (2004) and Sesar et al. (2006) in which the authors used the SDSS repeated imagings in combination with the Palomar Observatory Sky Survey (POSS) data to probe long-term QSO variability (up to $\sim$ 50 years), and constrained its timescale to be $\sim$ 1 year in the rest frame.

Normal "inactive" galaxies (for our purpose defined to be galaxies that are not Type 1 or Type 2 AGNs, or low-ionization nuclear emission regions (LINERS; Heckman 1980)) are not observed to be variable; and are generally not expected to be. For the continua of galaxies, the timescale of observation is negligible compared with that of stellar evolution (for solar-mass main sequence stars, lifetime $\approx 10^{10}$ years). For emission-line regions that arise from low-density environments and H II regions, similar arguments can be made to those for narrow-line regions, with the understanding that the electron density is likely to be lower ($n_e \sim$ 1–1000 cm^{-3}; Spitzer 1978).

The goal of this work is, therefore, to probe spectral variability of galaxies and narrow-line AGNs using the SDSS multiepoch observations. The SDSS data have the advantage of large sample size with the same spectrophotometric reduction, which is critical to our work because we expect any variability present in galaxies to be small (compared with the amplitude of the QSO UV-optical variability, for example). Several techniques are used to refine the spectroscopic calibration, including those by Wilhite et al. (2005). The resultant galaxy variability measurement is compared with that of stars and QSOs, independently analyzed in this work.

In Section 2 we discuss the samples used. In Section 3 we present the variability measure. In Section 4 we describe the refinement of the spectroscopic calibration. In Section 5 we present the galaxy continuum variability, and the emission line variability of the variable candidates based on the continuum. In Section 6 we present results on variability analyses on stars and QSOs as sanity checks. In Section 7 we summarize the results and discuss future work.

2. SAMPLES

As part of the SDSS (York et al. 2000), spectra are observed with fibers of 3″ diameter (corresponding to 0.18 mm at the focal plane for the 2.5 m, $f/5$ telescope, Gunn et al. 2006). The spectral resolution R is $\sim$ 1800 in the observed frame 3800–9200 Å. All sources are selected (or "targeted") from an initial imaging survey using the SDSS camera as described in Gunn et al. (1998) with the filter response curves as described in Fukugita et al. (1996), and using the imaging processing pipeline of Lupton et al. (2001). The astrometric calibration is described in Pier et al. (2003). The photometric system and calibration are described in Fukugita et al. (1996), Hogg et al. (2001), Smith et al. (2002), Ivezić et al. (2004), and Tucker et al. (2006). The targeting strategy for the multiobject spectrograph is described in Blanton et al. (2003).

We select our samples from the Data Release 6 (DR6; Adelman-McCarthy et al. 2008) of the SDSS. The galaxy sample is constructed from the SDSS Main Galaxy sample (Strauss et al. 2002) by selecting spectra which are both spectroscopically classified as galaxies, and rejecting spectra in which the redshift measurements failed or have not been made. The spectral classification (star, galaxy, QSO) is highly confident, with 98% of all the DR6 spectra having consistent classification between the spectro1d pipeline (SubbaRao et al. 2002) and the specBS pipeline (D. J. Schlegel et al. 2009, in preparation). From this sample, pairs of spectral observations are identified by matching sources in both R.A. and decl. to within 1″, and in redshift to within 0.01. Spectra at both epochs are required to have the same plate number but different dates of observations, given in Modified Julian Date (MJD) by the SDSS. The selection results in 23,330 pairs. The subsequent sample selections (mainly for the purpose of increasing the signal-to-noise, S/N, of the spectra) will be described in Sections 4 and 5. Table 1 lists the relevant spectroscopic plates and the corresponding number of galaxy spectra. The sample covers $\sim$ 3–700 days in the observed frame.

The spectroscopically classified galaxies selected above do not contain any strong (equivalent width, EW $>$10 Å, and $> 3\sigma$ detection in the height of the line) broad line (FWHM $>$1000 km s^{-1}; SubbaRao et al. 2002). The cutoff is below the traditional line-width selection for broad lines (Type 1) galaxies, where the width of permitted line(s) $>$ 2000 km s^{-1} (e.g., Komossa 2008). The sample therefore comprises galaxies of different eClass types (Connolly et al. 1995), and narrow-line AGNs. A potential contamination to our galaxy sample would be the narrow-line Seyfert 1 galaxies (Osterbrock & Pogge 1985, and references therein), expected to offer a direct view of the active nuclei (Antonucci 1993; Urry & Padovani 1995) and can be variable in the optical (Giannuzzo & Stirpe 1996; Peterson et al. 2000). Each of these spectra shows a broad component in Balmer emission line with FWHM $<$ 2000 km s^{-1}, and relatively weak [O III]λ5008. The reasons behind this potential contamination are twofold: firstly, the spectro1d pipeline fits to each line a single Gaussian that may underestimate the line width of the broad component in the case of a composite line which is made up of both the broad and narrow components, in particular when the broad one is relatively weak. Secondly, the FWHM of the broad component of both Hα and Hβ of a narrow-line Seyfert 1 can extend down to $\sim$ 500 km s^{-1} (Figure 4 of Zhou et al. 2006), falling within the galaxy spectral classification in the SDSS. However, we expect the number contribution of these objects to the whole DR6 galaxy+QSO sample to be small, $\sim$ 0.5%, with reference to Zhou et al. (2006) who used an upper limit of 2200 km s^{-1} in the broad component of Hα or Hβ emissions to search for narrow-line Seyfert 1 in the SDSS. Similarly, the Seyfert 1.8 and 1.9 (Osterbrock 1989), both of which show strong narrow components (relative to the broad ones, if available) in Hα and Hβ, can be variable in the optical (Goodrich 1989), and may be present in our galaxy sample as well. We note that the current analysis does not provide further separation of those from our emission-line galaxies, that calls for fitting of double Gaussian to each Balmer line, for example. The number contribution of these types to the full galaxy sample is expected to be small, $\sim$ 0.02% (Wang & Wei 2008). In this work, the fraction of the classified Seyfert 2 + star-forming + composite galaxies to the full sample of our galaxy spectral pairs is $\sim$ 14%; and that of all the eClass types, $\sim$ 22% (calculated from Table 4).

When constructing the stellar and QSO samples, the spectral pairs are selected similarly to the case of galaxies, except that they are spectroscopically classified as star and QSO, respectively. The targeting selection for spectroscopic observation of

Table 1
Spectroscopic Plates Used in the Analysis of Galaxies

Plate[a,b]	First Epoch MJD	Second Epoch MJD	Difference in MJD	Total Number of Pair[c]	Number of Pair[d]
266	51602	51630	28	447	356
279	51608	51984	376	430	361
282	51630	51658	28	346	278
284	51662	51943	281	425	336
285	51663	51930	267	417	317
291	51660	51928	268	444	344
296	51665	51984	319	448	364
297	51663	51959	296	453	369
300	51666	51943	277	386	288
301	51641	51942	301	370	282
304	51609	51957	348	398	317
306	51637	51690	53	435	352
309	51666	51994	328	371	287
340	51691	51990	299	385	302
348	51671	51696	25	313	240
351	51695	51780	85	395	311
385	51783	51877	94	326	259
390	51816	51900	84	392	313
394	51812	51913	101	347	267
404	51812	51877	65	421	335
406	51817	52238	421	319	239
410	51816	51877	61	309	243
411	51817	51873	56	398	318
412	51931	52258	327	396	306
413	51821	51929	108	351	274
414	51869	51901	32	383	299
415	51810	51879	69	366	277
416	51811	51885	74	332	259
418	51817	51884	67	367	285
419	51812	51879	67	355	293
422	51811	51878	67	465	375
425	51884	51898	14	370	290
437	51869	51876	7	304	235
440	51885	51912	27	425	331
483	51902	51942	40	324	247
547	51959	52207	248	347	288
588	52029	52045	16	435	344
594	52027	52045	18	355	285
616	52374	52442	68	450	349
640	52178	52200	22	405	323
644	52149	52173	24	408	339
662	52147	52178	31	455	358
712	52179	52199	20	216	131
790	52433	52441	8	402	323
803	52264	52318	54	430	355
804	52266	52286	20	422	354
810	52326	52672	346	502	360
814	52370	52443	73	363	279
820	52433	52438	5	307	242
960	52425	52466	41	427	354
972	52428	52435	7	417	345
978	52431	52441	10	328	262
1028	52562	52884	322	466	371
1034	52525	52813	288	471	385
1037	52826	52878	52	508	417
1291	52735	52738	3	421	337
1512	53035	53742	707	144	99
1782	53299	53383	84	457	373
2009	53857	53904	47	449	354
2351	53772	53786	14	332	259
...	...	...	...	23,330[e]	18,435[e]

Notes.
[a] There are 60 spectroscopic plates used, taken from the SDSS DR6.
[b] The plates 1664, 1905, 1907, 2075 (not listed in the table) are not used because the number of galaxy pairs is less than 10.
[c] The total number of galaxy pairs in a plate.
[d] The number of galaxy pairs with successful calibration refinement using SYS+BAND.
[e] The number of galaxy pairs summing over all plates, respectively.

QSOs in the SDSS is described in Richards et al. (2002). Each QSO spectrum classified (SubbaRao et al. 2002) has at least one strong line (see above for the galaxy classification) with FWHM >1000 km s^{-1}, and/or a Lyman alpha forest. Unlike the selection of the galaxies and the QSOs, no criterion is imposed on the quality of the redshift when selecting the stars. The upper bound of their distances is $cz = 450$ km s^{-1}, or $z = 0.0015$ (SubbaRao et al. 2002). The samples contain 9100 stellar pairs and 3205 QSO pairs ($0.08 < z < 3.51$), respectively.

The spectra are dereddened against Galactic extinction using the library written by Simon Krughoff[9], which adopts the SFD dust maps (Schlegel et al. 1998) and the extinction curve by O'Donnell (1994). Following the SDSS convention the spectra are expressed in vacuum wavelengths. Flux densities f_λ are expressed in 10^{-17} erg s^{-1} cm^{-2} Å^{-1}.

3. VARIABILITY AMPLITUDE: $F_{\rm var}$

We adopt the dimensionless variability measure, $F_{\rm var}$, for N-epoch repeated observations (e.g., Rodriguez-Pascual et al. 1997; Peterson 2001). It is a fractional root-mean-squared variability amplitude defined as

$$F_{\rm var} = \frac{\sqrt{\sigma^2 - \delta^2}}{\langle f \rangle}, \tag{1}$$

where σ^2 is the variance of the flux, δ^2 is the mean square uncertainty of the flux, and $\langle f \rangle$ is the mean flux

$$\sigma^2 = \frac{1}{N}\sum_{i=1}^{N}(f_i - \langle f \rangle)^2 \tag{2}$$

$$\delta^2 = \frac{1}{N}\sum_{i=1}^{N}\delta_i^2 \tag{3}$$

$$\langle f \rangle = \frac{1}{N}\sum_{i=1}^{N} f_i. \tag{4}$$

The numerator, proposed by Bonoli et al. (1979), was termed the square-root of the "excess variance" (Vaughan et al. 2003), in the sense that the flux uncertainty is subtracted in quadrature from the variability. In the calculation of the continuum $F_{\rm var}$ the wavelength intervals encompassing emission-line center wavelengths ± 280 km s^{-1} are excluded (using the vacuum wavelength values in the line list[10] adopted by the SDSS, and excluding the lines Ca K and H, Hδ, the G band around 4306 Å, Mgλ5177, Naλ5896, and the Ca II triplet that usually appear as absorptions). The mean square uncertainty for the spectrum at each epoch (δ_i^2 for a given i) is calculated by quadrature summation of the pipeline flux uncertainty per pixel, over all valid pixels. It is therefore a variance in flux based on photon statistics. A valid pixel is defined to be a pixel that is not flagged as bad. The flags are listed in Section 4.2. $F_{\rm var}$ is calculated in the observed frame with wavelengths 3900–8900 Å for each object and for all spectral types.

When calculating $F_{\rm var}$ for narrow-line AGNs, since any possible host-galaxy contribution is not explicitly subtracted from an observed spectrum, the full observed spectrum is used in calculating the denominator $\langle f \rangle$. As the numerator term "excess variance" does not contain the nonvariable host-galaxy contribution, the resultant $F_{\rm var}$ is therefore a lower limit on the AGN variability.

If the excess variance $\sigma^2 - \delta^2 < 0$, we assume the variability is zero for the object, but continue to include it in the analysis. In this work, $N = 2$. We note that any nonzero $F_{\rm var}$ is referred to as a "variability" measurement, regardless of the origin being physically interesting or otherwise.

4. REFINING SPECTROSCOPIC CALIBRATION

The principal steps in the spectrophotometric calibration of each spectrum in the SDSS are: a wavelength-dependent calibration using the observed standard stars on the same plate; and the tying of the absolute flux scale to the observed point-spread function (PSF) magnitudes of stars, on the same plate (Adelman-McCarthy et al. 2008). The resultant average uncertainty in the spectrophotometry for DR6 is 7% at observed frame wavelength 3800 Å (Adelman-McCarthy et al. 2008). As any variability in the sources from our sample is expected to be of low amplitude, the calibration of the pipeline spectra must be improved using the approaches described below.

4.1. Wavelength-dependent Correction

We adopt the method developed by Wilhite et al. (2005) to remove systematics which may be present in each pair of galaxy spectra taken on separate MJDs. Flux-density corrections as a function of the observed-frame wavelength in the range of 3900–8900 Å are calculated by a linear fit (tied to the origin) between the flux density (f_λ) of all the objects at epoch 2 (the later epoch) and those at epoch 1. This calculation results in a calibration spectrum for one plate. We adopt a slightly different methodology from Wilhite et al. (2005) in which stellar spectra in each plate were used. Our calibration spectrum per plate is calculated using all galaxies present in that plate, as we want to maximize the number of objects in generating the calibration spectrum and avoid potential systematic effects when applying point source calibration to extended sources. The underlying assumption is that the majority of the galaxies observed in a given plate are nonvariable in time across the two epochs. Even if the galaxies were in fact variable, the method is still applicable because the variable amplitude of several hundred galaxies is not expected to be in phase. An example calibration spectrum is plotted in Figure 1. Typically the calibration spectra are smooth. To focus on low-order corrections to the galaxy spectra, and to remove noise in the calibration spectrum, we follow Wilhite et al. (2005) and set the final calibration spectrum per plate as its fifth-order polynomial least-squares fit. By visual inspection this functional form works well in removing higher-order spurious spectral features.

When constructing the calibration spectrum we drop any plate in which there are less than 10 pairs of galaxy spectra. We then refine each and every spectrum present in a given plate by using the calibration spectrum, if available.

4.2. Wavelength-independent Correction

After removing wavelength-dependent systematics, each spectral pair can, in principle, be subjected to a wavelength-independent normalization in their flux densities. In order to obtain an accurate variability measurement of each spectral pair, the total continuum fluxes of the two spectra at a chosen common wavelength region are set equal. Specifically, for each pair the galaxy spectrum at the epoch of lower S/N is shifted in a

[9] The library is available from the author upon request.
[10] Stoughton et al. (2002).

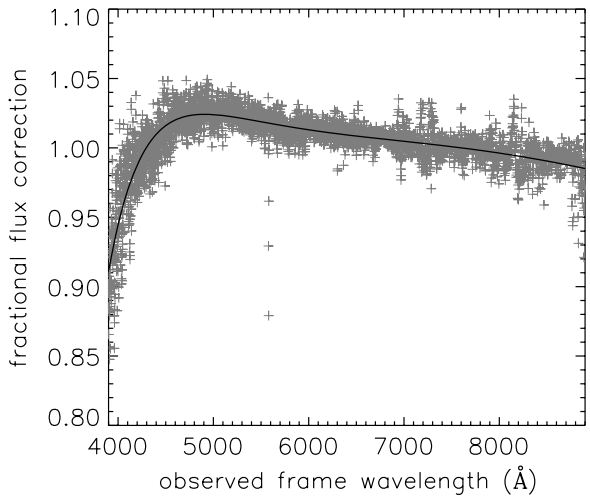

Figure 1. Calibration spectrum (gray crosses) of the spectroscopic plate 390 and its fifth-order polynomial fit (black line). The correction in flux density between two epochs is a function of the observed-frame wavelength.

wavelength-independent fashion according to

$$f_\lambda^{(\mathrm{low\,S/N})}(\mathrm{corrected}) = C_{\mathrm{band}}\, f_\lambda^{(\mathrm{low\,S/N})}(\mathrm{original}), \quad (5)$$

in which C_{band} is a constant for each spectral pair, calculated as

$$C_{\mathrm{band}} = F_{\lambda\in\mathrm{band}}^{(\mathrm{high\,S/N})} / F_{\lambda\in\mathrm{band}}^{(\mathrm{low\,S/N})}, \quad (6)$$

where $F_{\lambda\in\mathrm{band}}$ is the total flux in the rest-frame wavelength range (which is referred to as "rest-band" for convenience). In this work the rest-band is chosen to be 6450 Å ± 520 km s^{-1}, as such no prominent emission lines are present in the galaxy spectra.[11] Only the galaxy spectra in the first epoch are recalibrated because it is typically the existence of low S/N data that results in a second observation. The combined procedure of systematics removal and rest-frame band scaling is referred to "SYS+BAND" in the following discussion.

Given an initial sample (Section 2, 23,330 objects), we impose S/N cuts using the rest-band measures (or the [O III]λ5008 (vacuum) line, described later when we discuss absolute flux calibration). In this case we reject any spectral pair if there are one or more pixels flagged in either or both spectra in the wavelength region of interest, and we require the flux to be larger than zero at both epochs. The flags under consideration are NOPLUG, BADTRACE, BADFLAT, BADARC, MANYBADCOL, MANYREJECT, LARGESHIFT, FULLREJECT, SCATTERLIGHT, CROSSTALK, NOSKY, BRIGHTSKY, NODATA, COMBINEREJ, BADFLUXFACTOR, BADSKYCHI, and REDMONSTER. All of the spectral flux or S/N calculations in this paper are carried out with pixel-masking using these flags. After this S/N criteria, the number of objects in the galaxy sample is reduced to 18,435 (Table 1).

In Figures 2 and 3 we show the rest-frame galaxy spectra in two epochs from the SDSS pipeline and after the calibration refinement, respectively. Firstly, we note that the pipeline performs well, that the fractional difference between both epoch is about 10% at the shortest wavelength, which is sufficient for many spectral analyses involving emission or absorption lines. However, continuum residual in Figure 2 is present,

[11] When refining QSO spectra which are located at a wide range of redshift, an *observed frame* wavelength range 6450 Å ± 520 km s^{-1} is used.

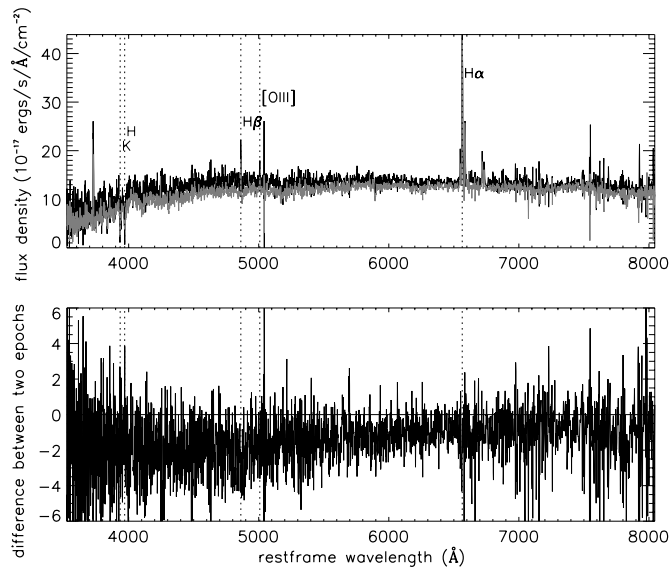

Figure 2. Example star-forming galaxy without any calibration refinement ($F_{\mathrm{var}} = 0.058$). Top: spectra at the first (black) and the second (gray) epoch. Bottom: difference spectrum.

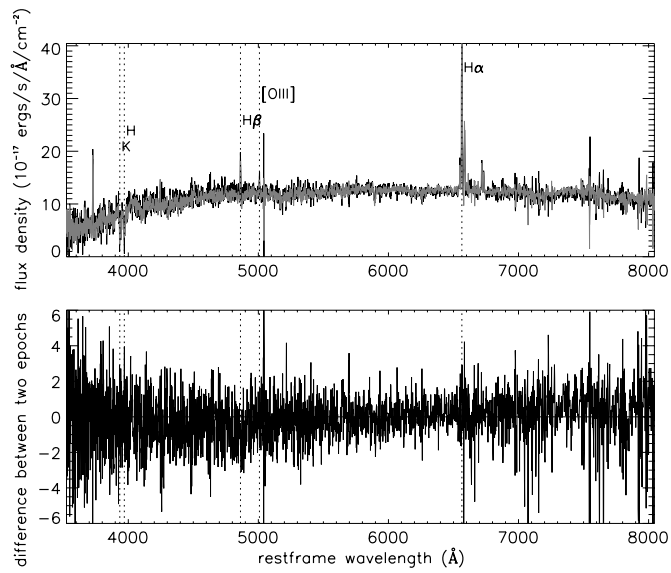

Figure 3. Same galaxy as in Figure 2, which shows zero continuum variability ($F_{\mathrm{var}} = 0$) after the SYS+BAND calibration refinement. Top: spectra at the first (black) and the second (gray) epoch. Bottom: difference spectrum.

which induces a variability ($F_{\mathrm{var}} = 0.058$). After the calibration refinement we are able to obtain a zero continuum variability.

For comparing with the rest-band scaling previously discussed, we also adopt the absolute flux calibration described in Peterson et al. (1998). In this procedure, the spectrum in the low S/N epoch in the duo is scaled wavelength-independently so that its total flux in [O III]λ5008 (vacuum) is the same as that of the spectrum in the high S/N epoch. The physical justification is that the [O III]λ5008 line generally appears as a narrow line arising from a low-density region, which is believed to be nonvariable in time (Peterson et al. 1995). We note that the average [O III] EW of galaxy spectra in the full DR6 catalog is a few Å, so for some objects mainly the continuum flux is measured and is expected to be nonvariable as well. The combined procedure of systematics removal and absolute [O III] calibration is called "SYS+O III" in the following. The region of influence is set to be 5008 Å ± 280 km s^{-1}.

Table 2
Statistics of $F_{\rm var}$ in Galaxies Using Different Calibration Refinements

Method	Mean[a]	σ_m	σ
No refinement[b]	0.020	0.0002	0.025
SYS+BAND	0.010	0.0001	0.009
SYS+BAND (280 km s^{-1})[c]	0.012	0.0001	0.011
SYS+O III	0.016	0.0001	0.015
SYS+BAND (RED galaxies)[d]	0.010	0.0001	0.009
SYS+BAND (BLUE galaxies)[d]	0.010	0.0001	0.009

Notes. There are 11,766 common spectral pairs in each of the calibration refinement approaches. Each spectrum is chosen to be refined successfully in each and every one of the above procedures. In principle, there can be more objects with successful refinement in each case.
[a] The statistics of $F_{\rm var}$ are calculated at spectral S/N $\geqslant$ 10: σ_m is the standard deviation of the mean of $F_{\rm var}$, σ is the one sigma sample scatter.
[b] The spectra are the direct output made available by the SDSS and no calibration refinement is done.
[c] Same as SYS+BAND (in which the rest-band considered is 6450 Å $\pm$ 520 km s^{-1}) but using 6450 Å $\pm$ 280 km s^{-1}.
[d] Same as SYS+BAND but using only the RED or the BLUE galaxies in calculating the calibration spectrum.

When judging which method performs better in analyzing spectral variability, we consider the better method to be the one which minimizes the mean, one standard deviation of the mean (σ_m) and the one standard deviation sample scatter (σ) of the variability at a fixed spectral S/N. These statistics for the galaxy sample by using the SYS+BAND, SYS+O III and other refinement methods are listed in Table 2. At S/N $\geqslant$ 10 the SYS+BAND method produces smaller mean and scatter in $F_{\rm var}$. The difference is not related to the difference in the width of the rest-band being used (520 km s^{-1} versus 280 km s^{-1}), as the SYS+BAND method is also re-performed using 6450 Å $\pm$ 280 km s^{-1}, the same width as in the SYS+O III method. These statistics remain lower in value than those in the SYS+O III even for this reduced interval. The result suggests that the [O III]λ5008 line in some spectra may be impacted by the effect of seeing so that the total observed line flux is different for the two epochs. The other possible reasons for this discrepancy are the total line flux is sampled at only a few wavelength bins in the medium resolution SDSS spectra, or the line may exhibit intrinsic variability.

To further test the method SYS+BAND, we divide the galaxy sample into RED and BLUE galaxies by using the eClass classification (described in Section 5.2.1). The RED spectra are defined as objects with classification parameter $\phi_{KL} \geqslant 0^\circ$, and the BLUE galaxies, $\phi_{KL} < 0^\circ$. For each plate, the calibration spectrum is calculated using only the RED or BLUE galaxies, which in turn is used to re-calibrate galaxies of all spectral types on the same plate. The purpose behind this is to determine whether the refinement method SYS+BAND would be biased by the presence of potentially different galaxy spectral types in the plate. We find that using a specific spectral type does not cause the variability statistics to change (Table 2). We therefore adopt SYS+BAND as the calibration method, and use all available galaxy spectral types when calculating the calibration spectrum throughout this work. The "before and after" of this approach is shown in Figure 4, where we see that the scatter in $F_{\rm var}$ versus S/N of our galaxy sample is reduced after the refinement. Comparing the average variability of our galaxy sample using the SYS+BAND approach with that from the original SDSS spectral reductions (Table 2), we find that the spectrophotometry is improved by a factor of 2.

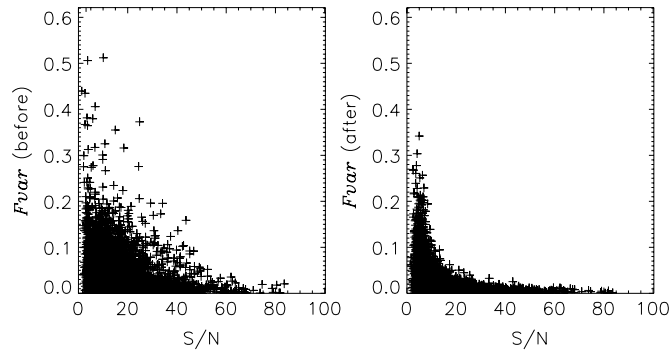

Figure 4. $F_{\rm var}$ vs. S/N of galaxy spectra before (left) and after (right) the SYS+BAND calibration refinement. The number of objects in each spectroscopic plate is listed in Table 1.

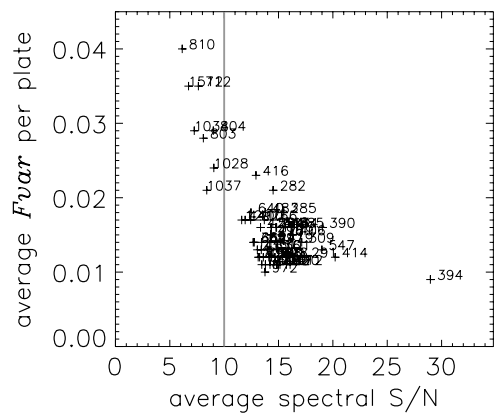

Figure 5. Average variability of galaxy spectra over a given spectroscopic plate plotted vs. the average spectral S/N. The spectra at S/N $\geqslant$ 10 are selected in the subsequent definition of variable and nonvariable candidates to minimize variation in $F_{\rm var}$ among plates.

4.3. Plate-to-Plate Difference

There are plate-to-plate differences seen in the above definitions of variable and nonvariable sources, that is, the best-fit coefficients in Equation (7) are in general plate dependent. In Figure 5 we show $\langle F_{\rm var}\rangle$ of the galaxy spectra versus average spectral S/N, per plate. The average $F_{\rm var}$ per plate is larger at lower overall spectral S/N, suggesting in those plates the variability measurement is likely affected by the presence of noise in the spectra. By dropping individual spectral pairs with spectral S/N < 10 at the second epoch, the average and the sample scatter in $F_{\rm var}$ are reduced to 0.010 and 0.003, respectively.

5. GALAXY VARIABILITY

5.1. Defining Variables

Following Wilhite et al. (2005), we define the variable candidates by objects having

$$F_{\rm var}({\rm S/N}) > {\rm b}_0 \exp\left(\frac{\rm S/N}{\rm b_1}\right) + {\rm b}_2. \quad (7)$$

The S/N of each spectrum is calculated in the second epoch and by using all of the valid pixels as defined in Section 4.2. The constants b_0, b_1, b_2 are determined by least-squares fitting the above exponential form to the binned data ($\langle$S/N$\rangle$, $\langle F_{\rm var}\rangle + n\,\sigma(F_{\rm var})$), where $\sigma(F_{\rm var})$ is one standard deviation of $F_{\rm var}$ in each bin, and for $n = 0, 1, 2, 3, 4$. Typically 10 bins in S/N are used.

Table 3
Upper Percentile of the Galaxy Variable Candidates[a]

Lower S/N	0	5	10	15	20
Upper S/N	5	10	15	20	40
Number[b]	11	102	246	206	86
Percentile[c]	1.53	1.89	3.92	6.26	3.44

Notes. In the galaxy sample using SYS+BAND refinement.
[a] The variable candidates are selected by $F_{\rm var} > (\text{mean} + 3\sigma)$ of $F_{\rm var}$ at a given spectral S/N.
[b] The number of variable candidates between the lower and upper S/N.
[c] The percentile of the corresponding number within a given S/N range.

The variable candidates (for galaxies, stars and QSOs) in this work are defined as objects with $> 3\sigma$ detection. We do not subdivide the distribution for detections greater than 4σ, though in the future we plan to explore in more detail the tail of the variable distributions. For comparison we have also defined variables as objects located in a fixed upper percentile of $F_{\rm var}$ in the plot $F_{\rm var}$ versus S/N. The $> 3\sigma$ cut is equivalent to a 2%–6% upper percentile for a given S/N (Table 3).

5.2. Continuum

To explore any dependence of spectral variability or repeatability on the spectral type of galaxies, we divide the galaxy sample using two different spectral classification schemes: eClass (Connolly et al. 1995) and the "BPT" diagrams or the Osterbrock diagrams (Baldwin et al. 1981; Veilleux & Osterbrock 1987). These two schemes are motivated by different spectral features. The eClass is a spectral type describing the steepness of the continuum slope and other higher-order spectral features by using a linear combination of several eigenspectra for each galaxy spectrum. The eClass parameters, ϕ_{KL} and θ_{KL}, are related to the coefficients in the eigenspectra expansion (called eigencoefficients), which are calculated by the Spectro1d pipeline in the SDSS. Specifically, the angle ϕ_{KL} correlates with the Hα emission EW (Madgwick et al. 2003) which is an indicator of star formation rate. The angle θ_{KL} discriminates galaxy spectra exhibiting post-starburst activities (Connolly et al. 1995; Yip et al. 2004).

On the other hand, the BPT diagrams separate the narrow-line AGNs from galaxies such as the star-forming galaxies by emission line ratios which indicate the physical conditions of gas inside the galaxies such as the electron density and the mean level of ionization (Osterbrock 1989). The objects in these two spectral classification schemes are not mutually exclusive. We hereafter present results on variability within both kinds of classification.

5.2.1. eClass

The spectral variability as a function of S/N per mean eClass galaxy type (Connolly et al. 1995) is shown in Table 4, and Table 5 for only the variable candidates. The mean eClass spectra are galaxy spectra where each is averaged over a nontrivial size of subspace of the two eClass parameters ϕ_{KL} and θ_{KL} (Yip et al. 2004). Limited by the number of spectral pairs, $\leqslant 3$ in types E or F, only the types A, B, C and D are considered in the variable candidates (Table 5). The continuum of the mean galaxy spectrum is reddest in the type A and bluest in the type D.

Firstly, we note that the average variability amplitude are consistent among different eClass types to within 1–2σ sample scatter. If we assume a priori that some populations of galaxies do not vary in time, then a spectral repeatability can be assigned to the population with the smallest mean and scatter in $F_{\rm var}$, that is, the mean eClass type B. The spectral features of this class are similar to the elliptical galaxies in the atlas of nearby galaxies by Kennicutt (1992). The repeatability, taken to be the average $F_{\rm var}$, is 0.010 or 1.0% in the observed-frame wavelength range 3900–8900 Å.

Table 4
Statistics of $F_{\rm var}$ in the Full Galaxy Sample

Type	Number [a,b]	Mean	σ_m	σ [a]
Seyfert 2	92	0.009	0.0008	0.008
Star-forming	1333	0.012	0.0003	0.011
Composite	314	0.010	0.0005	0.009
eClass A	729	0.010	0.0004	0.010
eClass B	919	0.010	0.0003	0.010
eClass C	587	0.011	0.0004	0.010
eClass D	483	0.012	0.0005	0.010
eClass E	3	0.024	0.0100	0.017
eClass F	5	0.044	0.0124	0.028
RED	9603	0.009	0.0001	0.009
BLUE	2705	0.012	0.0002	0.011

Notes. In the galaxy sample using SYS+BAND refinement.
[a] The number of spectra at S/N $\geqslant$ 10.
[b] We do not find any LINER (Heckman 1980) in our galaxy sample, using the classification criteria by Kewley et al. (2006, their Equation (15)).

Table 5
Statistics of $F_{\rm var}$ in the Galaxy Variable Candidates

Type	Number [a]	Mean	σ_m	σ [a]
Seyfert 2	5	0.026	0.0030	0.007
Star-forming	62	0.037	0.0023	0.018
Composite	13	0.031	0.0043	0.015
eClass A	34	0.031	0.0027	0.016
eClass B	45	0.031	0.0020	0.014
eClass C	37	0.030	0.0015	0.009
eClass D	18	0.034	0.0030	0.013
RED	388	0.028	0.0006	0.012
BLUE	154	0.034	0.0012	0.015

Notes. In the galaxy sample using SYS+BAND refinement.
[a] The number of spectra at S/N $\geqslant$ 10.

5.2.2. Emission-line Galaxies: Narrow-line AGN versus Star-forming

Emission-line galaxies are considered by using the BPT diagram, using the starburst theoretical modeling line by Kewley et al. (2006). We consider the types: Seyfert 2, star-forming, composite, and LINERs (Heckman 1980). We do not find any LINER in our galaxy spectral pairs, using the classification criteria by Kewley et al. (2006, their Equation (15)) which involved [O I]λ6302. We hereby consider the diagram $\log_{10}$([O III]/Hβ) versus $\log_{10}$([N II]/Hα) (Figure 5 of Baldwin et al. 1981).

In the first step of this analysis the EWs are taken from the SDSS reduction. Galaxies with any one of the four lines (Hβ at 4863 Å, [O III]λ5008, Hα at 6565 Å, [N II]λ6585) having rest-frame EW smaller than 1 Å are rejected (in the SDSS convention EW > 0 for emission lines); and at least a 2σ detection is required in each of the four lines. Rest-frame stellar absorption of the related hydrogen emission lines in the BPT diagram is corrected for by a constant increment of 1.3 Å (Hopkins et al. 2003; Miller et al. 2003). Any possible aperture effect on the emission lines is neglected in this paper, because the primary

Table 6
Difference in AB Synthetic Absolute Magnitude Between the Dim and Bright Phases in g, r, i Bands, for Variable Candidates

type	$\langle M_g \rangle$[a]	$\langle M_r \rangle$	$\langle M_i \rangle$	$\langle z \rangle$[b]	$\langle \Delta M_g \rangle$[c]	$\langle \Delta M_r \rangle$	$\langle \Delta M_i \rangle$	$\delta(\langle \Delta M_g \rangle)$[d]	$\delta(\langle \Delta M_r \rangle)$	$\delta(\langle \Delta M_i \rangle)$	$\sigma(\Delta M_g)$[e]	$\sigma(\Delta M_r)$	$\sigma(\Delta M_i)$
Seyfert 2	−20.57	−21.36	−21.30	0.14	0.07	0.05	0.05	0.26	0.12	0.20	0.01	0.03	0.03
Star-forming	−18.79	−19.37	−19.46	0.09	0.10	0.05	0.05	0.09	0.04	0.08	0.05	0.03	0.05
Composite	−19.79	−20.53	−20.53	0.11	0.09	0.04	0.03	0.19	0.08	0.13	0.05	0.02	0.03
eClass A	−20.70	−21.55	−21.25	0.15	0.08	0.05	0.06	0.11	0.05	0.85	0.04	0.04	0.05
eClass B	−20.12	−20.95	−20.74	0.13	0.09	0.05	0.04	0.10	0.04	4.82	0.03	0.03	0.03
eClass C	−19.95	−20.73	−20.81	0.12	0.09	0.04	0.04	0.12	0.05	0.08	0.03	0.02	0.03
eClass D	−18.18	−18.75	−18.91	0.07	0.09	0.04	0.06	0.16	0.07	0.12	0.05	0.02	0.06
RED	−20.14	−20.99	−20.91	0.13	0.08	0.04	0.05	0.03	0.01	3.16	0.04	0.03	0.04
BLUE	−19.27	−19.87	−19.89	0.10	0.09	0.05	0.05	0.06	0.03	0.05	0.05	0.03	0.05

Notes.
[a] The sample-averaged absolute AB magnitude in the dim phase. Unless otherwise specified, the terms "bright" and "dim" refer to the epoch among the two where the observed spectral flux is larger and smaller and do not necessarily imply an underlying physical mechanism.
[b] The sample average of the redshift.
[c] The sample average of the magnitude difference, $\Delta M_g = M_g(\text{dim}) - M_g(\text{bright})$, between the dim and bright phases.
[d] The uncertainty in the sample-averaged magnitude difference, by propagating the uncertainty in spectral flux density to that in magnitude, and then to the uncertainty of the sample-averaged magnitude difference.
[e] The 1σ sample scatter in the ΔM_g.

interest of this work is the comparison of line strength between two epochs, which is done using the same aperture for each object in each epoch and will only be subject to the difference in seeing. To correct on an object-by-object basis would require an assumption of an average line strength as a function of radius for each galaxy. Although the true line-flux correction of individual objects should depend on the distribution of the gas and its projected angle on the sky relative to the observational aperture, under the typical sky conditions in the SDSS observation (the median PSF width = 1″.4 in the r band; Figure 4 of Abazajian et al. 2003) and given the diameter of the fiber, the seeing-induced aperture correction factor to [O III] is close to unity, based on a nearby ($z = 0.009$) Seyfert 1 with a well resolved ($\sim 10''$) narrow-line region (Figure 3 of Wanders et al. 1992). This means that seeing-induced differences in the [O III] flux between any two epochs should be small. Further, the SDSS 3″ diameter fiber spectroscopy does not cause substantial aperture bias in classifying galaxy spectra based on emission lines (Miller et al. 2003).

In Table 4 we compare the variability amplitude between the star-forming galaxies and the narrow-line AGNs in the full galaxy sample, and Table 5 for the variable candidates. It is a little surprising that the average variability amplitude at S/N $\geqslant 10$ is 1.2% for the star-forming galaxies, slightly higher than that of the narrow-line AGNs, 0.9%. The difference is bigger than $1\sigma_m$ (i.e., the measurement of the $F_{\rm var}$ difference is reliable), but smaller than the 1σ sample scatter, indicating the $F_{\rm var}$ of both types are consistent with each other.

In Table 6 we show the average absolute AB magnitudes in g, r, and i bands of variable candidates in the dim phase, and the sample-averaged magnitude difference between the dim and bright phases, per spectral type. The magnitudes are calculated for each spectrum, by convolving each rest-frame-shifted spectrum with the SDSS filter response curves for extended sources at an airmass of 1.3 (Fukugita et al. 1996), and in the AB filter system (Oke & Gunn 1983). The average difference in the g-band magnitudes ranges from 0.07 to 0.10 mag depending on the spectral type, but they are consistent among different spectral types to within 1σ sample scatter of the magnitude difference, $\sigma(\Delta M)$, a measure of the sum of the sample scatters in both the distributions of M(dim) and M(bright). For the narrow-line AGNs, no obvious continuum variability is found (e.g., 0.07 ± 0.26 mag in the g band).

We note that the distribution of $F_{\rm var}$ in the full sample is non-Gaussian. Using the $> 3\sigma$ cut for the variable candidates, for a Gaussian distribution one would expect the ratio between the number of variable candidates and that of the whole sample to be

$$\frac{1 - \text{erf}(3/\sqrt{2})}{1 - \text{erf}(-\infty)}, \tag{8}$$

or 0.13 %, where erf(z) is the error function, and $1 - \text{erf}(z)$ is the complementary error function of the form $(2/\sqrt{\pi}) \int_z^\infty e^{-t^2} dt$. From Table 3, we see that typically at various S/N the $F_{\rm var}$ of the variable candidates span a longer tail (1.53%–3.44%).

5.2.3. Structure Function of the Continuum

The characteristic timescale of variability is usually studied by constructing the structure function (SF, e.g., Simonetti et al. 1985, Hughes et al. 1992, and references therein), the variability amplitude $F_{\rm var}$ as a function of time lag. Although no obvious continuum variability is found in our sample of galaxies on average, the SF is nonetheless constructed for the galaxy sample. Through the SF analysis, an absence of a timescale would be a cross-check of the lack of variability, and the comparison between the SF of stars and of QSOs (Section 6) with that of the galaxies can be carried out.

The rest frame SF, $F_{\rm var}$ versus $\Delta\tau_{\rm rest}$, of all galaxies in the galaxy sample is illustrated in Figure 6, where $\Delta\tau_{\rm rest} = \Delta\tau/(1+z)$, and z being the redshift of a given galaxy. The time lag $\Delta\tau$ is the difference between the two MJDs of observation, MJD(epoch 2)−MJD(epoch 1). No obvious timescale is seen in the above rest-frame SFs of galaxies for the 0–500 days (rest-frame) sampled. A similar conclusion is obtained when the fractional change in flux ($|\Delta f/f|$) is used instead of $F_{\rm var}$ (Figure 7), where Δf is the difference in the flux between two epochs, and f is the average flux over the two epochs.

An exponential function of the form

$$F_{\rm var} = a\,(1 - b\,e^{-\Delta\tau_{\rm rest}/\tau_s}) \tag{9}$$

is fitted to each structure function, where τ_s is the characteristic variability timescale. Typically, a structure function where

Table 7
Best-fit Characteristic Variability Timescale

Type	Zero Point $F_{\rm var}$[a]	τ_s (year)[b]	Asymptotic $F_{\rm var}(\Delta\tau_{\rm rest}\rightarrow\infty)$	Reduced χ^2	Range in $\Delta\tau_{\rm rest}$ (day)
QSO	0.012 ± 0.003	0.4 ± 1.0	0.022 ± 0.002	0.04	0–300
star	0.010 ± 0.069	11.2 ± 6.3	0.035 ± 0.035	3.41	0–710
galaxy	0.009 ± 0.162	8.5 ± 1.6	0.025 ± 0.081	19.52	0–500

Notes.
[a] $F_{\rm var}$ at zero time lag.
[b] Characteristic variability timescale in the rest frame.

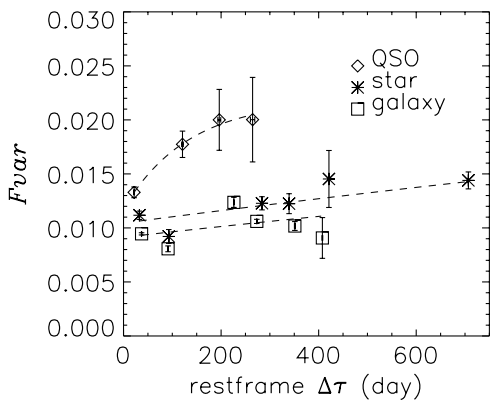

Figure 6. Rest-frame structure function of the QSOs, stars and galaxies. Only spectra with S/N $\geqslant$ 10 are shown. Error bar is $1\sigma_m$ for each axis. The dotted line shows the best-fit structure function of an exponential functional form in $\Delta\tau_{\rm rest}$.

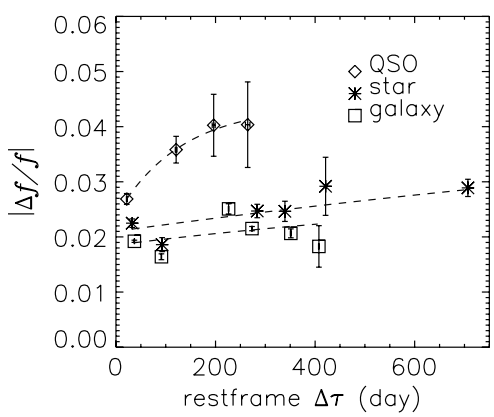

Figure 7. Rest-frame structure function. Same as Figure 6 except that the fraction change in total flux $|\Delta f/f|$ is used instead of $F_{\rm var}$.

$b = 1$ is considered (e.g., Bonoli et al. 1979; Trevese et al. 1994). Firstly we relax b to accommodate the nonzero variability at zero time lag, obvious in Figure 6. This can be attributed to the repeatability of the continuum variability measurement (Section 5.2.1) in eClass Type B, where the mean $F_{\rm var}$ is 0.010 or 1.0%. The best-fit τ_s for the galaxies is $\sim$ 10 years (Table 7). The uncertainty of this timescale is large ($\sim$ 2 years, with a reduced χ^2 of 20) because the duration of the observation is much shorter than the best-fit τ_s.

We then consider a typical $b = 1$ structure functional form at Equation (9). By assuming $F_{\rm var}$ at the zero time lag ($F_{\rm var}(0)$) (the noise) is uncorrelated with the intrinsic $F_{\rm var}$(the signal), one can obtain the intrinsic $F_{\rm var}$ by subtracting $F_{\rm var}(0)$ from the total $F_{\rm var}$ in a quadrature fashion. The resultant structure function is shown in Figure 8, and the best-fit variability timescales in

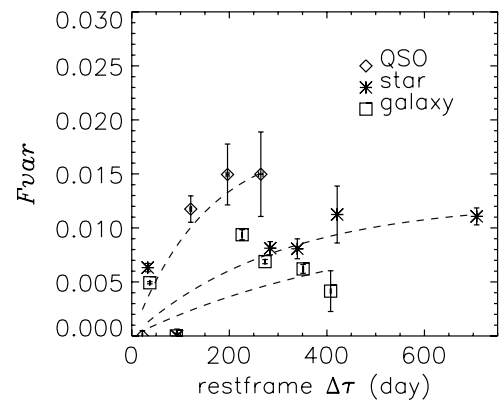

Figure 8. Rest-frame structure function of the QSOs, stars and galaxies. Different from Figure 6 which shows the total variability, here the variability at the zero time lag is quadrature subtracted, respectively in each spectral type. Only spectra with S/N $\geqslant$ 10 are shown. Error bar is $1\sigma_m$ for each axis. The dotted line shows the best-fit structure function of an exponential functional form in $\Delta\tau_{\rm rest}$.

Table 8, where $F_{\rm var}(0)$ is taken to be the minimum of the total $F_{\rm var}$. The large best-fit χ^2 in stars and galaxies implies that the best-fit variability timescales are quite uncertain. A longer duration of observation would be ideal to improve the structure function.

5.3. Emission Lines

The BPT diagram is constructed for the variable candidates to explore the narrow emission-line variability. Again the emission-line ratios $\log_{10}$([N II]/Hα) versus $\log_{10}$([O III]/Hβ) are considered.

In measuring the EW of an emission line, we fit to a given continuum-subtracted spectrum a single Gaussian function. The continuum is estimated by non-negative least square fitting (Lawson & Hanson 1974), provided by Dobos et al. (2006) who used the Bruzual & Charlot (2003) stellar population 1 Å resolution models. In this way, the stellar absorption in the Balmer lines is implicitly taken into account in the best-fit stellar continuum. In measuring the uncertainty of an EW, the following steps are performed. Firstly, the uncertainty in the luminosity densities of the stellar continuum of the spectrum is calculated by using $\delta f_\lambda^c = \delta f_\lambda$, where δ denotes the uncertainty of the continuum flux density f_λ^c and of the observed spectrum f_λ. The uncertainty in each EW is calculated to be $\sum_{\lambda_R}\delta(f_\lambda - f_\lambda^c)/f_\lambda^c\, d\lambda$, where λ_R is the region of influence of the emission lines, taken to be around the line center $\pm$280 km s^{-1}. Finally, the uncertainty in each of the line ratios $\log_{10}$([N II]/Hα) and $\log_{10}$([O III]/Hβ) is propagated by using common error propagation formula.

The line ratios between the dim and bright phases of sources are found to be located very closely on the BPT diagram,

Table 8
Best-fit Characteristic Variability Timescale, After Quadtrature Subtraction of Variability at Zero Time Lag

Type	τ_s (year)[a]	Asymptotic $F_{\rm var}(\Delta\tau_{\rm rest} \rightarrow \infty)$	Reduced χ^2	Range in $\Delta\tau_{\rm rest}$ (day)
QSO	0.4 ± 0.0	0.018 ± 0.005	13.10	0–300
star	0.8 ± 0.0	0.012 ± 0.003	49.71	0–710
galaxy	1.4 ± 0.0	0.011 ± 0.018	501.97	0–500

Notes. [a] Characteristic variability timescale in the rest frame.

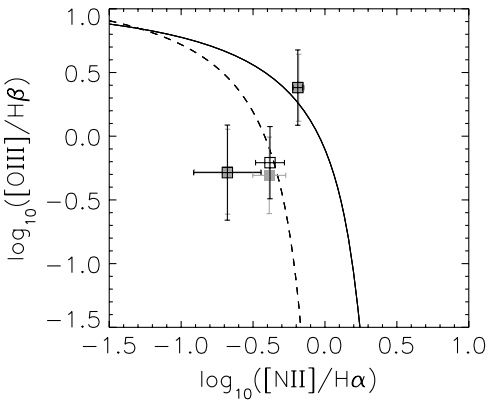

Figure 9. BPT diagram of the continuum variable candidates. The object type from the lowest to the highest [N II]/Hα value is: star-forming, composite, and Seyfert 2. In each duo the filled square represents the average line ratios of the brighter objects, and the empty square for the dimmer ones. The solid and dashed lines respectively define the Seyfert 2 and star-forming galaxies as given by Kewley et al. (2006). The line ratios in all object types do not show substantial change between both epochs. The error bar represents the 1σ sample scatter in each phase.

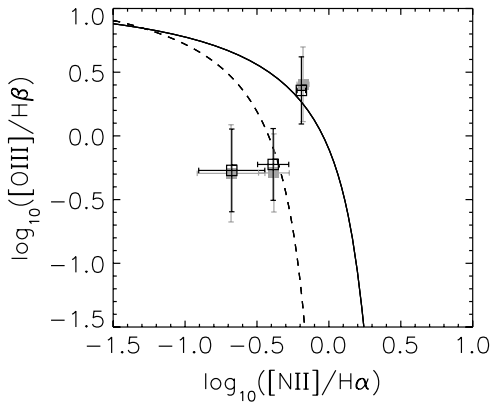

Figure 10. Similar to Figure 9, but in each duo the filled square represents the average line ratios of the first epoch, and the empty square for the latter epoch. The error bar represents the 1σ sample scatter in each epoch.

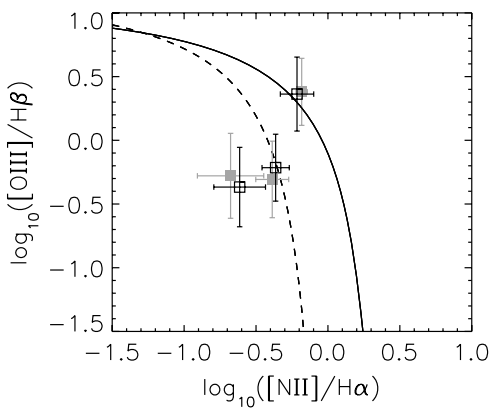

Figure 11. Similar to Figure 9, but in each duo the filled square represents the average line ratios of the continuum variable candidates, and the empty square for the nonvariable ones. Line ratios in both cases are from the bright phase. The error bar represents the 1σ sample scatter.

as shown in Figure 9. The emission-line ratios and their uncertainties for various object types are given in Table 9. The uncertainty in the flux measurement is small, for example in the star-forming galaxies, which indicates a reliable line measurements. For both line ratios the difference between the dim and bright phases is typically comparable to the 1σ sample scatter in the line-ratio difference (i.e., the last two columns of Table 9). This is true for all of the object types considered, meaning we find no evidence of narrow emission-line-ratio variability which is above 1σ level. When dividing the line-ratio measurements by the first and second epoch (Figure 10) instead of the dim and bright phases, we also see no difference between the two that is larger than 1σ. Further, the line ratios of the variable candidates and the nonvariable candidates (Figure 11) do not show substantial difference in the BPT diagram, true for all of the emission-line galaxy types.

The above analyses are also repeated with the intrinsically dereddened spectra using the best-fit color excess ($E(B-V)$) (C. W. Yip et al. 2009, in preparation), by the non-negative least square fitting of stellar population models on the SDSS DR6 galaxies (Dobos et al. 2006). Expectedly, each of the average line ratios remains unchanged to the 1σ level (not shown), because the central wavelengths of the two lines for a given line ratio are close and is thus insensitive to dust reddening.

6. COMPARISON WITH STAR AND QSO

To evaluate further the performance of the calibration refinement, we refine the calibration in stellar and QSO spectra in a spectroscopic plate using calibration spectrum constructed from galaxies of the same plate. The procedure is described in Section 4.

6.1. Variability in SDSS Stellar and QSO Spectra

Table 10 lists the statistics of $F_{\rm var}$ in our sample of the SDSS stellar spectra. The improvement in the repeatability after the SYS+BAND refinement is a factor of 3. The average $F_{\rm var}$ of stars is found to be slightly higher than that of the galaxies.

Table 11 lists the statistics of $F_{\rm var}$ in our sample of the SDSS QSO spectra. The QSOs are located within a redshift range of 0.08–3.51 with an average of 1.16. Upon the SF analysis the characteristic timescale of the QSOs is found to be 0.4 ± 1.0 years (Table 7), which agrees with the timescales commonly found in the literature (e.g., Cristiani et al. 1996; Ivezić et al. 2004; Vanden Berk et al. 2004) for the UV-optical variability.

The comparison between the SF of galaxies, stars, and QSOs in Figures 6 and 7 shows that $F_{\rm var}$(QSO) $>$ $F_{\rm var}$(star) $>$ $F_{\rm var}$(galaxy).

Table 9
BPT Line-ratio Difference Between Dim and Bright Phases, for Variable Candidates

Type	$\langle \Delta\log_{10}([\mathrm{N\,II}]/\mathrm{H}\alpha)\rangle$[a]	$\langle \Delta\log_{10}([\mathrm{O\,III}]/\mathrm{H}\beta)\rangle$	$\sigma(\Delta\log_{10}([\mathrm{N\,II}]/\mathrm{H}\alpha))$[b]	$\sigma(\Delta\log_{10}([\mathrm{O\,III}]/\mathrm{H}\beta))$
Seyfert 2	0.02 ± 0.03	0.06 ± 0.08	0.03	0.03
Star-forming	0.09 ± 0.01	0.16 ± 0.03	0.17	0.21
Composite	0.03 ± 0.03	0.11 ± 0.09	0.03	0.08
eClass C	0.17 ± 0.05	0.47 ± 0.12	0.18	0.43
eClass D	0.07 ± 0.02	0.15 ± 0.06	0.08	0.17

Notes.
[a] The sample-averaged line ratio. The quoted uncertainty is the uncertainty in the spectral flux measurement.
[b] The 1σ sample scatter in the line-ratio difference between dim and bright phases.

Table 10
Statistics of F_{var} in Stars

Method	Mean	σ_m	σ
No refinement	0.035	0.0011	0.053
SYS+BAND	0.012	0.0003	0.013

Notes. See the caption in Table 2 for the meaning of the statistics. There are 2379 common spectral pairs in each of the refinement approaches. The statistics of F_{var} are calculated at spectral S/N $\geqslant$ 10.

Table 11
Statistics of F_{var} in QSOs

Method	Mean	σ_m	σ
No refinement	0.036	0.0012	0.034
SYS+BAND	0.015	0.0005	0.014

Notes. See the caption in Table 2 for the meaning of the statistics. There are 766 common spectral pairs in each of the refinement approaches. The statistics of F_{var} are calculated at spectral S/N $\geqslant$ 10.

6.2. Cross Match with GCVS

The full samples of galaxies, stars, and QSOs are matched with the General Catalogue of Variable Stars (GCVS; Kholopov et al. 1999, Vol. I–III and references therein) as an assessment to the definition of variability. The R.A. and decl. are both matched to within 1″, respectively.

Table 12 shows the objects that exist in both the GCVS and our samples. As expected, all of the matched objects are spectroscopically classified as stars by the SDSS. Three of the five GCVS stars are defined in this work to be variable candidates ($> 3\sigma$ detection), hence a completeness of 60% when using two-epoch observations to infer the stellar variability.

The above indicates that the variability of stars and galaxies in this study could in principle be limited by the small number of epochs, also pointed out by Ivezić et al. (2003), and that the defining of variable stars by more than 3σ over the average in the variability may need to be adjusted. The fact that more than half of the variable candidates are real variable stars according to the GCVS shows that the calibration refinement is successful in selecting those objects.

6.3. Cross Match with SDSS Southern Stripe

Our full samples of galaxies, stars and QSOs are also cross-matched with the variable catalog constructed by Sesar et al. (2007) based on the SDSS repeated imaging (the Stripe 82). The data cover more observation epochs (from 4 to 28, with an average of 9), useful for determining the completeness of our variable candidates based on 2 epochs. The matched objects are found to be either stars or QSOs in the SDSS spectral classification, as Sesar et al. (2007)'s catalog is for unresolved objects only. In Table 13 the matched stars are listed. Five out of 22 sources matched to the SDSS variable catalog are defined to be variable stars in this work ($> 3\sigma$ detection), implying a 23% completeness when using two-epoch observations to infer the stellar variability.

For QSOs, because more than 300 matches are found, only the number of found objects is summarized in Table 14, along with our detection significance as variable candidates. About 10% of the objects are considered to be real variables in this work. If some of the narrow-line AGNs do vary in time, the completeness of the variable candidates from our current two-epoch sample may be as low as 10%.

7. SUMMARY

We probe the spectroscopic variability in the galaxies and narrow-line AGNs in the optical wavelengths using multiepoch observations in the SDSS. In order to detect the expected low amplitude of variability, we compare several approaches to refine the spectrophotometric calibration in the SDSS. The final calibration, in terms of the mean and the standard deviation of the variability in our galaxy sample, is a factor of 2 better than the official SDSS reductions.

Our sample of galaxy pairs spans in the rest frame $\sim$ 110 days on average, with a maximum of $\sim$ 700 days. The average change in the narrow-line AGN continuum flux, when converted to synthetic AB absolute magnitudes using the SDSS filters, is 0.07 ± 0.26 mag in the synthetic g band, where the uncertainty is propagated from the uncertainty in the spectral flux measurement. The fact that no obvious continuum variability is found is consistent with the expectation from the AGN unified model (Antonucci 1993; Urry & Padovani 1995), in which some of the light-emitting (in our context, continuum-generating) structures in a narrow-line AGN, such as the accretion disk, are obscured by a dusty torus. Hence, any variability in such structures (compare the UV-optical variability in QSOs in the timescale of one year) is not observed. This also provides an empirical evidence for modeling the continua of narrow-line AGNs using stellar population models (e.g., Kauffmann et al. 2003; Hao et al. 2005). Further, if we use this continuum variability measurement to set an upper limit on the AGN activities, then the ratio between the flux of any varying spectral component, presumably related to AGN activities, and that of the host galaxy is at most $\sim$ 30%.

By comparing the narrow emission-line ratios $\log_{10}([\mathrm{N\,II}]/\mathrm{H}\alpha)$ and $\log_{10}([\mathrm{O\,III}]/\mathrm{H}\beta)$ between the defined dim and bright phases in the continuum variable candidates, we find no evidence for their variability to be substantially larger than the 1σ sample scatter in the line-ratio difference. This is consistent with the

Table 12
Matched Objects Between GCVS[a] and Our Samples

R.A.[b] (degree)	Decl.[b] (degree)	SpecClass[c]	S/N	$\Delta\tau$[d]	Difference[e] in g	Difference in r	Difference in i	$F_{\rm var}$	nSigma[f]
218.750940	−0.768439	1	20.4	53	0.13 ± 0.49	−0.05 ± 0.30	−0.09 ± 0.41	0.017	1
118.540000	42.817851	1	39.0	7	−0.02 ± 0.26	0.00 ± 0.16	0.00 ± 0.21	0.005	0
119.352760	43.207637	1	43.0	7	0.05 ± 0.23	0.01 ± 0.16	−0.02 ± 0.22	0.011	3
120.915900	42.512477	1	46.5	7	−0.23 ± 0.20	−0.03 ± 0.13	0.08 ± 0.18	0.051	4
133.434070	57.811289	1	52.2	40	0.16 ± 0.18	0.06 ± 0.12	0.00 ± 0.18	0.045	4

Notes.
[a] The General Catalogue of Variable Stars (Kholopov et al. 1999).
[b] Given in J2000.
[c] All of the matched objects are stars according to the SDSS spectral classification.
[d] The time lag $\Delta\tau$ is the difference between the two MJDs of observation, MJD(epoch 2)−MJD(epoch 1).
[e] The difference in magnitude between two epochs.
[f] The detection significance as a variable candidate, derived from this work.

Table 13
Matched Objects Between SDSS Stripe 82 Variable Catalog[a] and Stars in This Work

R.A. (degree)	Decl. (degree)	SpecClass	S/N	Number of obs[a] in r	$\Delta\tau$	Difference in g	Difference in r	Difference in i	$F_{\rm var}$	nSigma
356.032540	1.027191	1	18.2	10	94	0.03 ± 1.64	0.01 ± 0.45	0.00 ± 0.49	0.003	0
356.151320	0.303432	1	9.1	12	94	−0.01 ± 2.13	−0.02 ± 0.68	−0.04 ± 0.73	0.007	0
356.171110	−1.220269	1	26.8	10	94	0.08 ± 0.53	0.00 ± 0.28	−0.07 ± 0.37	0.006	0
354.635580	0.856453	1	7.9	10	94	0.02 ± 1.28	−0.02 ± 0.94	−0.09 ± 1.68	0.039	1
12.348661	−0.299891	1	52.6	8	101	0.01 ± 0.23	0.00 ± 0.15	0.00 ± 0.23	0.000	0
13.369355	−0.722569	1	45.5	8	101	−0.13 ± 0.35	0.01 ± 0.19	0.05 ± 0.27	0.025	1
31.675864	0.988745	1	17.0	14	65	−0.01 ± 0.60	0.00 ± 0.35	0.01 ± 0.53	0.001	0
36.891406	0.437566	1	11.7	14	421	0.03 ± 0.79	0.03 ± 0.58	0.02 ± 0.97	0.013	0
35.787734	0.959517	1	25.6	14	421	−0.06 ± 0.44	−0.03 ± 0.26	0.01 ± 0.37	0.015	2
36.347691	0.660534	1	20.4	13	421	−0.04 ± 0.57	−0.03 ± 0.33	−0.03 ± 0.47	0.015	2
44.620576	−0.609703	1	14.3	14	61	0.18 ± 0.74	0.01 ± 0.45	−0.09 ± 0.71	0.036	4
44.322878	0.785284	1	13.2	14	61	−0.14 ± 0.73	−0.01 ± 0.44	0.06 ± 0.68	0.031	4
46.057464	−1.220639	1	29.6	12	56	−0.16 ± 0.32	−0.03 ± 0.20	0.07 ± 0.29	0.032	4
48.387960	0.715234	1	17.0	14	108	−0.07 ± 0.56	−0.02 ± 0.35	0.03 ± 0.58	0.014	1
49.984166	−0.044137	1	8.6	14	108	−0.12 ± 1.16	−0.01 ± 0.79	0.05 ± 1.39	0.030	0
51.883714	0.064299	1	54.1	12	32	−0.40 ± 0.19	−0.05 ± 0.12	0.15 ± 0.17	0.085	4
52.295747	0.603985	1	20.9	12	32	−0.08 ± 0.62	−0.01 ± 0.34	0.04 ± 0.49	0.015	2
52.476904	0.389118	1	45.5	14	32	0.02 ± 0.28	0.00 ± 0.17	0.00 ± 0.24	0.006	0
51.602434	0.674580	1	45.2	14	20	0.01 ± 0.24	0.01 ± 0.16	−0.04 ± 0.21	0.007	4
43.924804	−0.542138	1	2.8	14	707	−0.10 ± 4.41	0.15 ± 2.26	0.17 ± 3.21	0.017	0
44.201206	0.013831	1	19.2	14	707	−0.15 ± 1.10	−0.01 ± 0.30	0.03 ± 0.30	0.011	0
44.918114	0.758511	1	6.3	12	707	−0.14 ± 2.89	−0.17 ± 0.98	−0.28 ± 1.13	0.100	2

Notes. See also captions in Table 12.
[a] Given by Sesar et al. (2007).

common view in which the narrow-line emissions in the AGNs are generated from low-density clouds. For example, an electron density $n_e \sim 1,000\ {\rm cm}^{-3}$ gives rise to a hydrogen recombination time ~ 100 years, which is typically much longer than the duration of the observation.

We found no evidence of continuum variability in galaxies of eClass types A, B, C, D that is larger than the variability uncertainty. This agrees with the expectation that stellar light dominates their continuum, as in the narrow-line AGNs.

We tabulate the upper limits of both the continuum and emission-line variability as a function of spectral type, using the classification schemes eClass and the BPT diagram. These values can serve as a sanity check for researchers who study variability for other sources.

7.1. Variability in Classification

There were few attempts in examining the galaxy classification from the point of view of variability. A recent work by Brunzendorf & Meusinger (2001) suggested variability is an efficient method to find narrow-line AGN. However, this promising result was not subsequently confirmed by the authors (Meusinger & Brunzendorf 2002). Our result on narrow emission-line ratios being nonvariable seems to agree with the latter claim made by the authors.

Table 14
Matched Objects Between SDSS Stripe 82 Variable Catalog[a] and QSOs in This Work

nSigma[b]	Number of Objects	Percentage
0	231	67.3
1	45	13.1
2	33	9.6
3	10	2.9
4	24	7.0

Notes.
[a] Given by Sesar et al. (2007).
[b] The detection significance as a variable candidate, derived from this work.

7.2. Next Steps

So far we have focused on the average variability properties of the galaxies and narrow-line AGNs. We are investigating, on the object-to-object basis, any dramatic variation in spectral features or types.

We thank Brian Wilhite, David Turnshek, and Julian Krolik for discussions. We thank Brigitte König, Amy Kimball, and Scot Kleinman for discussions on variable stars. We thank Ani Thakar for discussions on SDSS databases. We thank the referee for helpful suggestions and discussions on narrow-line Seyfert 1 galaxies. A.S.S., R.F.G.W., T.B., and C.W.Y. acknowledge support through grants from the W. M. Keck Foundation and the Gordon and Betty Moore Foundation, to establish a program of data-intensive science at the Johns Hopkins University. A.J.C. acknowledges partial support from the NSF ITR award 0851007. L.D. and I.C. acknowledge support from grants MSRC-2005-038, NAP-2005/KCKHA005, and MRTN-CT-2004-503929.

Funding for the SDSS and SDSS-II has been provided by the Alfred P. Sloan Foundation, the Participating Institutions, the National Science Foundation, the U. S. Department of Energy, the National Aeronautics and Space Administration, the Japanese Monbukagakusho, the Max Planck Society, and the Higher Education Funding Council for England. The SDSS Web site is http://www.sdss.org/.

The SDSS is managed by the Astrophysical Research Consortium for the Participating Institutions. The Participating Institutions are the American Museum of Natural History, Astrophysical Institute Potsdam, University of Basel, University of Cambridge, Case Western Reserve University, the University of Chicago, Drexel University, Fermilab, the Institute for Advanced Study, the Japan Participation Group, Johns Hopkins University, the Joint Institute for Nuclear Astrophysics, the Kavli Institute for Particle Astrophysics and Cosmology, the Korean Scientist Group, the Chinese Academy of Sciences (LAMOST), Los Alamos National Laboratory, the Max-Planck-Institute for Astronomy (MPIA), the Max-Planck-Institute for Astrophysics (MPA), New Mexico State University, Ohio State University, the University of Pittsburgh, University of Portsmouth, Princeton University, the United States Naval Observatory, and the University of Washington.

REFERENCES

Abazajian, K., et al. 2003, AJ, 126, 2081
Adelman-McCarthy, J. K., et al. 2008, ApJS, 175, 297
Antonucci, R. 1993, ARA&A, 31, 473
Aretxaga, I., Cid Fernandes, R., & Terlevich, R. J. 1997, MNRAS, 286, 271
Baldwin, J. A., Phillips, M. M., & Terlevich, R. 1981, PASP, 93, 5
Blanton, M. R., Lin, H., Lupton, R. H., Maley, F. M., Young, N., Zehavi, I., & Loveday, J. 2003, AJ, 125, 2276
Bonoli, F., Braccesi, A., Federici, L., Zitelli, V., & Formiggini, L. 1979, A&AS, 35, 391
Bono, G., Trevese, D., & Turatto, M. 2003, Mem. Soc. Astron. Ital., 74, 1004
Brunzendorf, J., & Meusinger, H. 2001, A&A, 373, 38
Bruzual, G., & Charlot, S. 2003, MNRAS, 344, 1000
Connolly, A. J., Szalay, A. S., Bershady, M. A., Kinney, A. L., & Calzetti, D. 1995, AJ, 110, 1071
Cristiani, S., Trentini, S., La Franca, F., Aretxaga, I., Andreani, P., Vio, R., & Gemmo, A. 1996, A&A, 306, 395
de Vries, W. H., Becker, R. H., & White, R. L. 2003, AJ, 126, 1217
Dobos, L., Budavari, T., Csabai, I., & Szalay, A. 2008, Astronomical Spectroscopy and Virtual Observatory Proceedings of the EURO-VO Workshop held 2007, March 21–23, Villa franca del Castillo, Spain, ed. M. Guainazzi & P. Osuna (Noordwijk: ESA), 79
Fukugita, M., Ichikawa, T., Gunn, J. E., Doi, M., Shimasaku, K., & Schneider, D. P. 1996, AJ, 111, 1748
Giannuzzo, E. M., & Stirpe, G. M. 1996, A&A, 314, 419
Goodrich, R. W. 1989, ApJ, 340, 190
Guainazzi, M., Matt, G., Antonelli, L. A., Fiore, F., Piro, L., & Ueno, S. 1998, MNRAS, 298, 824
Gunn, J. E., et al. 1998, AJ, 116, 3040
Gunn, J. E., et al. 2006, AJ, 131, 2332
Hao, L., et al. 2005, AJ, 129, 1783
Hawkins, M. R. S. 1993, Nature, 366, 242
Heckman, T. M. 1980, A&A, 87, 152
Hogg, D. W., Finkbeiner, D. P., Schlegel, D. J., & Gunn, J. E. 2001, AJ, 122, 2129
Hopkins, A. M., et al. 2003, ApJ, 599, 971
Hughes, P. A., Aller, H. D., & Aller, M. F. 1992, ApJ, 396, 469
Ivezić, Ž., et al. 2003, Mem. Soc. Astron. Ital., 74, 978
Ivezić, Ž., et al. 2004, Astron. Nachr., 325, 583
Ivezić, Ž., et al. 2004, in IAU Symp. 222, The Interplay Among Black Holes, Stars and ISM in Galactic Nuclei, ed. T. Storchi-Bergmann, L. C. Ho, & H. R. Schmitt (Dordrecht: Kluwer), 525
Jang, M. 2001, Ap&SS, 275, 209
Kauffmann, G., et al. 2003, MNRAS, 346, 1055
Kawaguchi, T., Mineshige, S., Umemura, M., & Turner, E. L. 1998, ApJ, 504, 671
Kennicutt, R. C., Jr. 1992, ApJS, 79, 255
Kewley, L. J., Groves, B., Kauffmann, G., & Heckman, T. 2006, MNRAS, 961
Kholopov, P. N., et al. 1999, VizieR Online Data Catalog, 2214, 0
Komossa, S. 2008, RevMexAA Conf. Ser., 32, 86
Lawson, C. L., & Hanson, R. J. 1974, Solving Least Square Problem (Englewood Cliffs, NJ: Prentice-Hall)
Lupton, R., Gunn, J. E., Ivezić, Z., Knapp, G. R., & Kent, S. 2001, in ASP Conf. Ser. 238, Astronomical Data Analysis Software and Systems X, ed. F. R. Harnden, Jr., F. A. Primini, & H. E. Payne (San Francisco, CA: ASP), 269
Madgwick, D. S., Somerville, R., Lahav, O., & Ellis, R. 2003, MNRAS, 343, 871
Mateos, S., Barcons, X., Carrera, F. J., Page, M. J., Ceballos, M. T., Hasinger, G., & Fabian, A. C. 2007, A&A, 473, 105
Meusinger, H., & Brunzendorf, J. 2002, A&A, 390, 439
Miller, C. J., Nichol, R. C., Gómez, P. L., Hopkins, A. M., & Bernardi, M. 2003, ApJ, 597, 142
Mueller, M., Madejski, G. M., Done, C., & Zycki, P. T. 2003, BAAS, 35, 637
O'Donnell, J. E. 1994, ApJ, 422, 158
Oke, J. B., & Gunn, J. E. 1983, ApJ, 266, 713
Osterbrock, D. E. 1989, Astrophysics of Gaseous Nebulae and Active Galactic Nuclei, (Sausalito, CA: University Science Books)
Osterbrock, D. E., & Pogge, R. W. 1985, ApJ, 297, 166
Pereyra, N. A., Vanden Berk, D. E., Turnshek, D. A., Hillier, D. J., Wilhite, B. C., Kron, R. G., Schneider, D. P., & Brinkmann, J. 2006, ApJ, 642, 87
Peterson, B. M. 2000, in Advanced Lectures on the Starburst-AGN Proc. Conf. Held in Tonantzintla, Puebla, Mexico, 26–30 June, 2001, ed. I. Aretxaga, D. Kunth, & R. Mjica (Singapore: World Scientific), 3
Peterson, B. M., McHardy, I. M., & Wilkes, B. J. 2000, New Astron. Rev., 44, 491
Peterson, B. M., Pogge, R. W., Wanders, I., Smith, S. M., & Romanishin, W. 1995, PASP, 107, 579
Peterson, B. M., Wanders, I., Bertram, R., Hunley, J. F., Pogge, R. W., & Wagner, R. M. 1998, ApJ, 501, 82
Pier, J. R., Munn, J. A., Hindsley, R. B., Hennessy, G. S., Kent, S. M., Lupton, R. H., & Ivezić, Ž. 2003, AJ, 125, 1559
Richards, G. T., et al. 2002, AJ, 123, 2945
Rodriguez-Pascual, P. M., et al. 1997, ApJS, 110, 9
Schlegel, D. J., Finkbeiner, D. P., & Davis, M. 1998, ApJ, 500, 525
Sesar, B., et al. 2006, AJ, 131, 2801
Sesar, B., et al. 2007, AJ, 134, 2236
Simonetti, J. H., Cordes, J. M., & Heeschen, D. S. 1985, ApJ, 296, 46
Smith, J. A., et al. 2002, AJ, 123, 2121
Spitzer, L. 1978, Physical Processes in the Interstellar Medium (New York: Wiley-Interscience), 333
Stalin, C. S., Gopal-Krishna, S. R., & Wiita, P. J. 2004, MNRAS, 350, 175
Stoughton, C., et al. 2002, AJ, 123, 485
Strauss, M. A., et al. 2002, AJ, 124, 1810
SubbaRao, M., Frieman, J., Bernardi, M., Loveday, J., Nichol, B., Castander, F., & Meiksin, A. 2002, Proc. SPIE, 4847, 452
Tohline, J. E., & Osterbrock, D. E. 1976, ApJ, 210, L117
Trevese, D., Kron, R. G., Majewski, S. R., Bershady, M. A., & Koo, D. C. 1994, ApJ, 433, 494

Trippe, M. L., Crenshaw, D. M., Deo, R., & Dietrich, M. 2008, AJ, 135, 2048
Tucker, D. L., et al. 2006, Astron. Nachr., 327, 821
Urry, C. M., & Padovani, P. 1995, PASP, 107, 803
Vanden Berk, D. E., et al. 2004, ApJ, 601, 692
Vaughan, S., Edelson, R., Warwick, R. S., & Uttley, P. 2003, MNRAS, 345, 1271
Veilleux, S., & Osterbrock, D. E. 1987, ApJS, 63, 295
Wanders, I., Peterson, B. M., Pogge, R. W., Derobertis, M. M., & van Groningen, E. 1992, A&A, 266, 72
Wang, J., & Wei, J. Y. 2008, ApJ, 679, 86
Wilhite, B. C., Vanden Berk, D. E., Brunner, R. J., & Brinkmann, J. V. 2006, ApJ, 641, 78
Wilhite, B. C., Vanden Berk, D. E., Kron, R. G., Schneider, D. P., Pereyra, N., Brunner, R. J., Richards, G. T., & Brinkmann, J. V. 2005, ApJ, 633, 638
Winkler, H., Glass, I. S., van Wyk, F., Marang, F., Jones, J. H. S., Buckley, D. A. H., & Sekiguchi, K. 1992, MNRAS, 257, 659
Yip, C. W., et al. 2004, AJ, 128, 585
York, D. G., et al. 2000, AJ, 120, 1579
Zhou, H., Wang, T., Yuan, W., Lu, H., Dong, X., Wang, J., & Lu, Y. 2006, ApJS, 166, 128